Non-linear dynamics of toroidicity-induced Alfven eigenmodes on NSTX

M. Podestà 1), R. E. Bell 1), N. A. Crocker 2), E. D. Fredrickson 1), N. N. Gorelenkov 1), W. W. Heidbrink 3), S. Kubota 2), B. P. LeBlanc 1), R. White 1), H. Yuh 4)

1) Princeton Plasma Physics Laboratory, Princeton NJ 08543 - USA

2) University of California Los Angeles, CA 90095, USA

3) University of California Irvine, CA 92697, USA

4) Nova Photonics, NJ 08543, USA

E-mail contact of main author: mpodesta@pppl.gov

Abstract. The National Spherical Torus Experiment (NSTX, [M. Ono *et al.*, Nucl. Fusion **40**, 557 (2000)]) routinely operates with neutral beam injection as the primary system for heating and current drive. The resulting fast ion population is super-Alfvénic, with velocities $1 < v_{fast}/v_{Alfven} < 5$. This provides a strong drive for toroidicity-induced Alfvén eigenmodes (TAEs). As the discharge evolves, the fast ion population builds up and TAEs exhibit increasing bursts in amplitude and down-chirps in frequency, which eventually lead to a so-called TAE avalanche. Avalanches cause large ($\lesssim 30\%$) losses over ~ 1 ms, as inferred from the neutron rate. The increased fast ion losses correlate with a stronger activity in the TAE band. In addition, a $n = 1$ mode with frequency well below the TAE gap appears in the Fourier spectrum of magnetic fluctuations during avalanche events. The non-linear coupling between modes, which leads to enhanced fast ion transport during avalanches, is investigated.

1. Introduction and experimental setup

The non-linear dynamics resulting from the coupling of multiple toroidicity-induced Alfvén eigenmodes (TAEs) is believed to represent one of the main loss mechanisms for fast ions in ITER [1]. Major consequences of enhanced losses are a decreased fusion efficiency and possible damage to in-vessel structures. It is therefore important to understand this phenomenon in order to limit, or avoid, its effects. Bursts of TAE activity with duration ~ 1 ms are commonly observed in neutral beam-heated plasmas on the National Spherical Torus Experiment (NSTX) [2]. A prompt depletion of up to 30% of the confined fast ion population correlates with single events [3][4]. The TAE bursts are thought to be caused by an enhanced coupling between unstable modes. The experimental results presented in this paper are consistent with a quadratic coupling between TAEs with consecutive toroidal numbers during their bursty, explosive growth.
NSTX operates at toroidal field $3.5 - 5.5$ kG, with typical density $3 - 10 \times 10^{19}$ m^{-3} and temperature $T_e \approx T_i \lesssim 1.5$ keV. Neutral beam (NB) injection is the primary system for heating and current drive. The total available power is $P_{NB} = 7$ MW at injection energy $E_{inj} = 60 - 90$ keV. The resulting fast ion population is super-Alfvénic with velocities $1 < v_{fast}/v_{Alfven} < 5$. Fast ions provide the drive for a variety of Alfvénic instabilities, including TAEs [5]. The latter have typical toroidal mode number up to $n = 8$ and
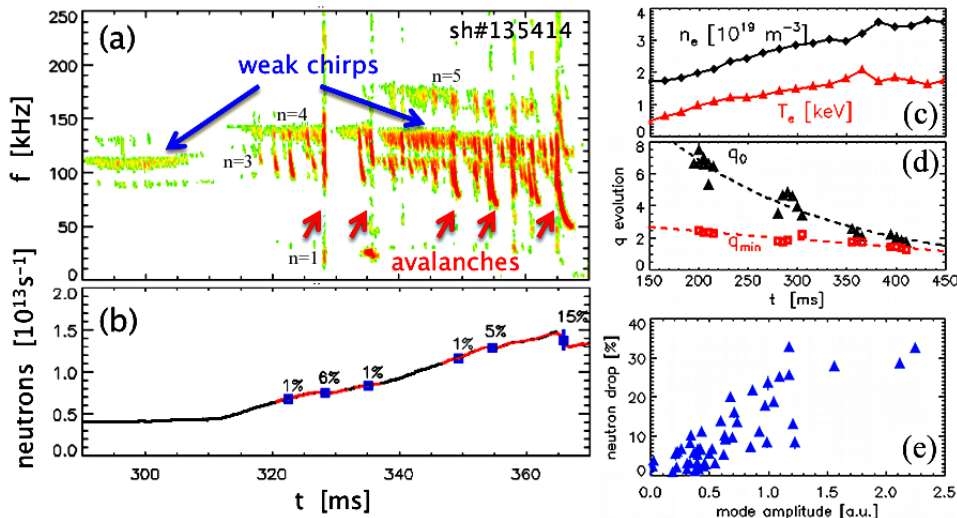
FIG. 1. (a) Spectrogram of magnetic field fluctuations from Mirnov coils. (b) Neutron drops associated with TAE avalanches. (c) Evolution of density and electron temperature at the magnetic axis. (d) Evolution of the central and minimum values of the safety factor, q_0 and q_{min}, reconstructed from four (nominally identical) discharges. (e) Relative drop in the neutron rate vs. mode amplitude during TAE bursts for a set of similar discharges.

frequency $60 < f < 250$ kHz. An example is shown in Fig. 1a for a L-mode deuterium plasma with 1.5 MW of injected NB power. The reversed-shear safety factor profile, $q(R)$, evolves in time. Its minimum, q_{min}, decreasese from 4 to ≈ 2 during the time of interest (Fig. 1d). Since no direct measurement of $q(R)$ through Motional Stark Effect (MSE) was available for this discharge, the safety factor is reconstructed *a posteriori* from similar discharges where MSE was available through the Grad-Shafranov equilibrium code LRDFIT, developed at PPPL by J. E. Menard. Weak variations of the mode amplitude, measured by Mirnov coils, correlate with frequency variations < 10 kHz for $t < 310$ ms. Later in time, the modes exhibit larger bursts in amplitude and frequency down-chirps > 10 kHz, which eventually lead to a so-called TAE *avalanche* [4]. Avalanches cause fast ion losses up to $\sim 30\%$ over ~ 1 ms [3], as inferred from the neutron rate, *cf.* Fig. 1b-e. The drop in the neutron rate *vs.* mode amplitude, integrated over $15 < f < 250$ kHz, is illustrated in Fig. 1e for a set of similar discharges. As expected, the losses increase with the mode amplitude [4][6]. In addition, activity with $n = 1$ and $f \sim 25$ kHz (i.e. well below the TAE gap), along with a weaker $n = 2$ harmonic at twice that frequency, is detected during TAE bursts. This fluctuation has a duration comparable with that of the avalanches. The temporal correlation with TAE bursts suggests that the $n = 1$ fluctuation may have a role in the fast ion loss process, as discussed in the next Sections.

2. Experimental results

2.1 General characteristics of TAE dynamics

For the type of discharges investigated in this work, TAEs exhibit common, general features that do not vary substantially from shot to shot. A salient feature is the almost constant frequency separation between peaks with consecutive n's. This suggests that the modes share a common frequency in the plasma frame, f_0^{TAE} [7]:

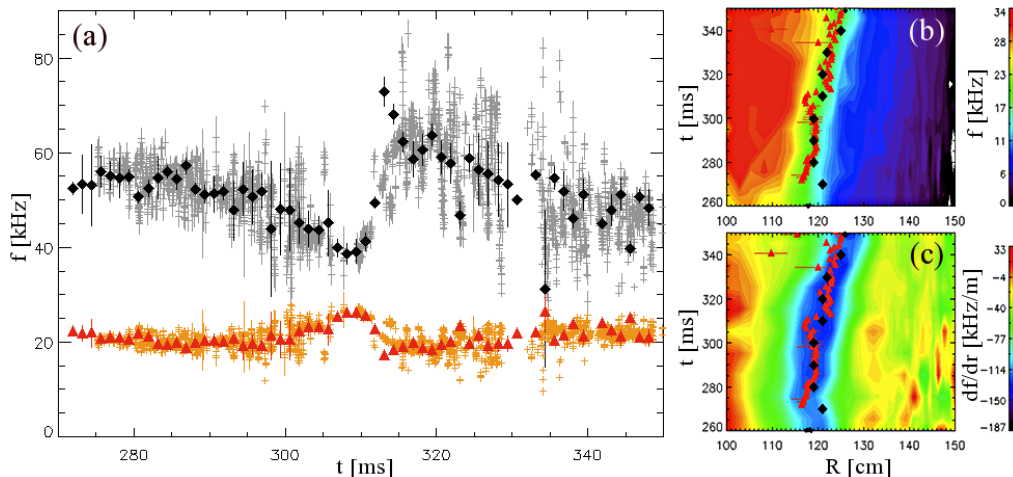$$f_{lab,n}^{TAE} = f_0^{TAE} + n\, f_{Doppler}^{TAE} \tag{1}$$

FIG. 2. (a) Calculated f_0^{TAE} and $f_{Doppler}^{TAE}$ from Eq. 1. Black symbols are the results from Fourier analysis, grey crosses (with associated error bars) are from time-domain analysis. (b,c) Toroidal rotation and toroidal rotation shear profiles. The symbols indicate the radius R^{TAE} at which $f_{Doppler}^{TAE}$ equals the toroidal rotation (red triangles) and the location of steepest fast ion density gradient (black diamonds).

where $f_{lab,n}^{TAE}$ is the frequency for the toroidal mode number n as measured in the laboratory frame and $f_{Doppler}^{TAE}$ the Doppler shift caused by plasma rotation. In practice, a gaussian fit of the peaks in the FFT spectra from 1.25 ms time windows is first used to determine the center frequency and frequency spread of the different modes. Then, a linear fit based on Eq. 1 provides the values of f_0^{TAE} and $f_{Doppler}^{TAE}$. The results as a function of time are reported in Fig. 2a. $f_{Doppler}^{TAE}$ evolves slowly in time, except for a jump at $t \approx 310$ ms which is also observed in f_0^{TAE}. The jump correlates with a qualitative transition in the mode dynamics from quasi-stationary to a bursting/chirping regime. As a speculation, we observe that the mode structure and its (poloidal) harmonic composition may be changing, for example because of the evolution of the q-profile, and the different mixture of the poloidal harmonics of each mode is favoring its bursting character. In addition, the fast ion population is also increasing, as deduced by the rise in the neutron rate (Fig. 1b), indicating that the mode's drive may also be different for the two phases. Although the change in regime is observed in all discharges, not all of them show this sudden frequency variation.

As a further step, the radius R^{TAE} at which the plasma rotation f_{rot} (from charge-exchange recombination spectroscopy measurements of carbon rotation [8]) matches $f_{Doppler}^{TAE}$ is calculated and compared with other quantities, such as the location of steepest fast ion density gradient and of maximum rotation shear (Fig. 2b-c). In using the condition $f_{rot}(R^{TAE}) = f_{Doppler}^{TAE}$, the diamagnetic contribution to $f_{Doppler}^{TAE}$ [7] is $\lesssim 1$ kHz and is neglected. Also, the differential rotation between impurity and main ions [9] is neglected and the measured f_{rot} is used as rotation of the main ion species. The radii R^{TAE} and of the steepest fast ion gradient are approximately equal and show a similar temporal evolution [10]. The same position also corresponds to the location of largest rotation shear. Although the high shear does not affect the macroscopic mode dynamics (see Ref. [10]), it implies that small changes in R^{TAE} may lead to relatively large variations of $f_{lab,n}^{TAE}$ due to different Doppler shifts experienced by the modes, see below.
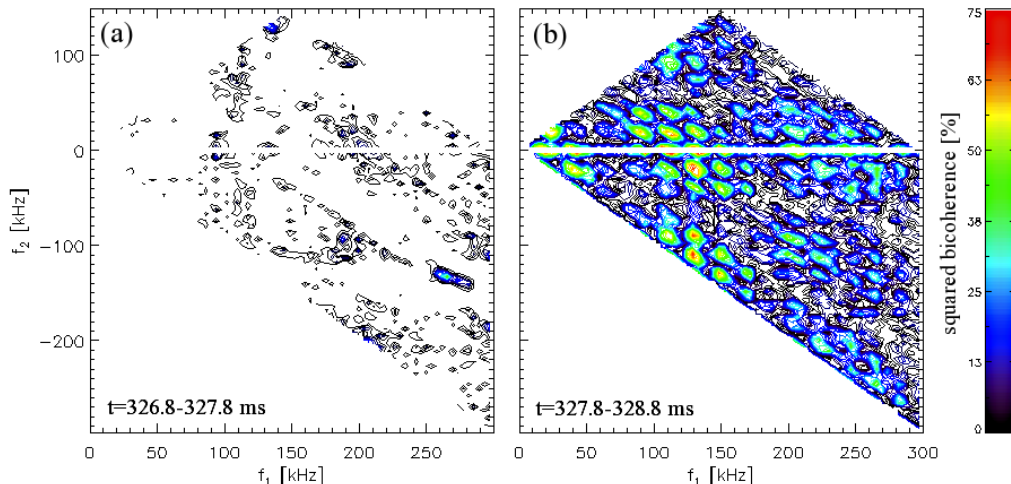
FIG. 3. *Average squared bicoherence from* 11 *Mirnov coils' signal for the discharge shown in Fig. 1 before (a) and during (b) a TAE burst at* $t \approx 328$ *ms. Data collected at 4 MHz sampling rate from a 1 ms time window are FFT analyzed with* 512 *frequency points. The higher bicoherence in (b) means more efficient coupling during the burst between frequency pairs* (f_1, f_2). *Sum and difference interactions appear in the top* $(f_2 > 0)$ *and bottom* $(f_2 < 0)$ *panel. The noise level in the bicoherence results is below* 10% *for both time intervals.*

The small error bars in the fit of f_0^{TAE} and $f_{Doppler}^{TAE}$ indicate that Eq. 1 describes well the frequency evolution over time scales $\gtrsim 1$ ms. The mechanism through which TAEs with different n's lock on a similar frequency are not yet clear. At present, it can be excluded that the modes are harmonics of a fundamental TAE mode or that they couple through a stationary low frequency mode, as was observed in Ref. [7]. The sub-millisecond dynamic is more complex. Each mode usually chirps independently of the others. The largest bursts represent an exception, in that most of the modes seem to lock onto a similar dynamic. For short time windows, the procedure illustrated above to find f_0^{TAE} and $f_{Doppler}^{TAE}$ gives more scattered results (Fig. 2). Nevertheless, two features emerge for the largest bursts: (i) $f_{Doppler}^{TAE}$ increases by a few kHz's, meaning that R^{TAE} moves inward (up-hill along the toroidal rotation profile); (ii) the frequency down-chirp in the laboratory frame is almost entirely ascribed to a down-chirp of f_0^{TAE}. A more complete description of the TAE dynamic during a burst requires a different analysis, as explained in the following paragraphs.

2.2 Verification of the conditions for mode coupling

The presence of mode-mode interactions is first investigated through *bicoherence* [11] which quantifies the degree of correlation between triplets of modes via a phase-weighted average of the complex Fourier bispectrum, normalized to the spectral amplitude. The bicoherence calculated before a TAE burst (Fig. 3a) is vanishing for small amplitude oscillations, indicating a weak or null coupling between modes which, nevertheless, still exhibit a bursting/chirping character. Conversely, values up to 75% are obtained during the burst for frequencies corresponding to the TAEs (Fig. 3b) and to the modes at $f < 60$ kHz and $f > 160$ kHz. Because of its limitations in temporal resolution and the lack of statistics for events of short duration, Fourier analysis has limited use to study the evolution of the mode coupling process during single bursts (100's of microseconds). An
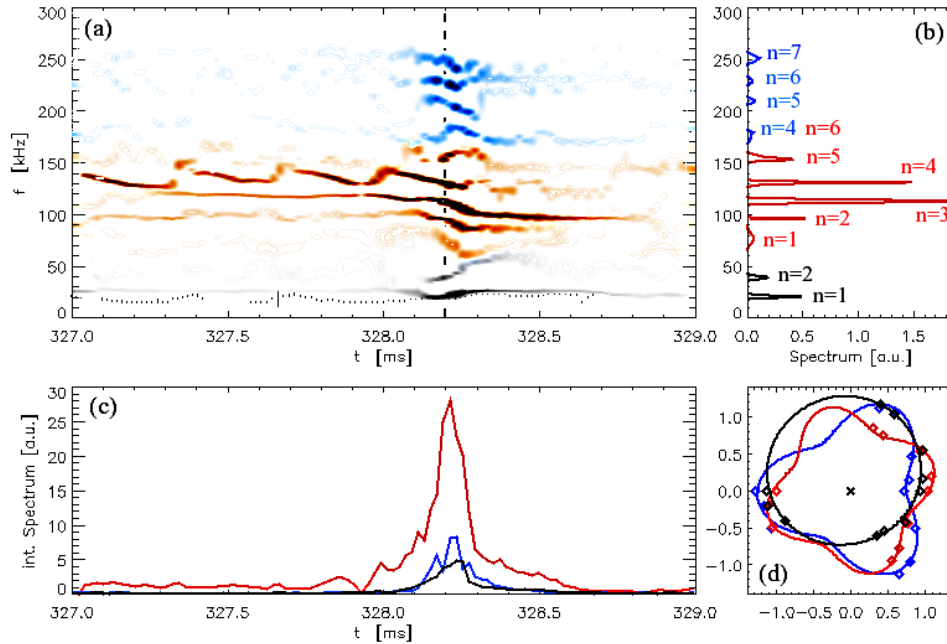
FIG. 4. (a) Spectrogram from time-domain analysis of the primary TAEs (red) and the low (black) and high (blue) frequency modes resulting from quadratic interactions. The dotted line is $f_{Doppler}^{TAE}$ from Eq. 1. (b) Spectrum at $t = 328.2$ ms, corresponding to the maximum TAE activity. (c) Amplitude for the three classes of modes integrated over the corresponding frequency range. (d) Mode amplitude from 11 Mirnov coil sensors distributed toroidally for the dominant $n = 3, 4$ TAEs and for the low-frequency $n = 1$ mode at $t = 328.2$ ms.

analysis in the time domain is instead used here. The analysis is performed as follows. Signals are band-pass filtered around the mode frequencies to obtain the fluctuations, $\dot{s}_n(t)$ ($n = 1, 2, \dots$), for each mode number n. The sum and difference of signals from sensors toroidally displaced 180° apart are used to further separate modes with even and odd mode number. The B-field fluctuation signals, $s_n(t)$, are calculated by integrating $\dot{s}_n(t)$ via software. The evolution of frequency and amplitude of the modes, f_n and A_n, are then obtained from the peak-to-peak amplitude and separation of the resulting (sinusoidal) signals s_n, each representing a mode with a specific frequency and toroidal mode number. Figure 4 shows the results of such analysis for a TAE burst at $t \sim 328.2$ ms. Before the burst only the *primary* TAEs are detected, with dominant $n = 3, 4$. The frequency of the two modes varies in time, but with no obvious correlation up to ≈ 328 ms. Then, their amplitude increases (Fig. 4c) and other modes are clearly observed at higher and lower frequencies, filling up the frequency spectrum up to 250 kHz. A progression in the toroidal mode number with frequency is present for each group of modes (primaries, low and high frequency), with a fixed separation between subsequent n's (Fig. 4b). The latter coincides with the frequency of the lowest frequency $n = 1$ mode.

From a simple model based on bilinear interactions between pairs of modes, the resulting fluctuation can be reconstructed as

$$\dot{s}_{n_3} = < c_{(n_1, n_2)} \, s_{n_1} s_{n_2} >_{f_{n_3}} \;\; ; \;\; n_3 = n_1 \pm n_2 \, , \; f_{n_3} = f_{n_1} \pm f_{n_2} \qquad (2)$$

where the right-hand side is filtered around the frequency f_{n_3} and the dot indicates a time derivative. Note that s_{n_2} is the complex conjugate of the true signal for difference interactions. $c(n_1, n_2)$ represents a (complex) coupling coefficient. For the real measured
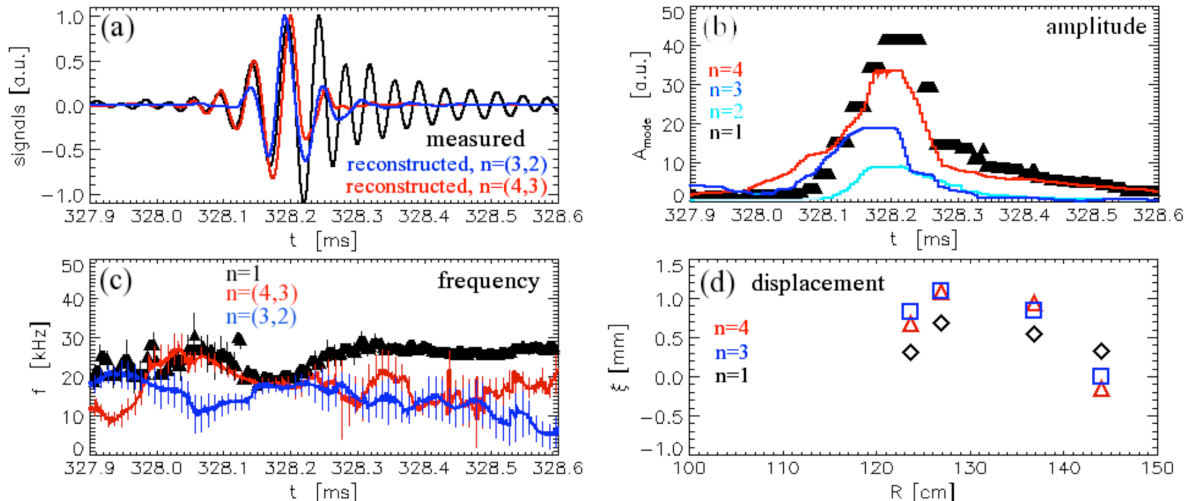
FIG. 5. (a) $n = 1$ *signal as measured and reconstructed from a simple model based on a bilinear interaction between* $n = (4, 3)$ *and* $n = (3, 2)$ *modes. (b) Amplitude of* $n = 1 \ldots 4$ *modes. (c) Evolution of* $n = 1$ *frequency and difference frequency between* $n = (4, 3)$ *and* $n = (3, 2)$ *modes for the discharge shown in Fig. 1a. (d) Reflectometer measurements of the radial displacement associated with* $n = 1, 3, 4$ *modes. Data from discharge no. 135414.*

signals, $s_n \rightarrow \Re\{s_n\}$ ($\Re\{\ldots\}$ is the real part) and a phase shift $\phi \neq 0$ exists between left- and right-hand sides of Eq. 2. The measured and reconstructed $\dot{s}_{n=1}(t)$ signals, shown in Fig. 5a-b, are consistent with this model for the pairs $n = (4, 3)$ and $n = (3, 2)$ and a phase shift of $180°$. The $n = 1$ oscillation amplitude grows at the same rate as the $(4, 3)$ and $(3, 2)$ bilinear terms, then decays when the amplitude of (at least one of) the pump TAEs vanishes, or the frequency match condition is no longer satisfied. A similar temporal evolution, but with a phase shift $\phi \sim 90°$, is observed for fluctuations resulting from *sum* interactions between the dominant modes. The frequency f_1 overlaps with the difference $f_4 - f_3$ and, later in time, with $f_3 - f_2$ (Fig. 5c). When that happens, the mode amplitude first increases rapidly, then decays again as the condition is no more satisfied. The frequency match for mode-mode coupling is therefore transiently verified, as shown in Fig. 5c for the reconstructed $n = 1$ amplitude according to Eq. 2. Figure 5d shows the displacement measured through reflectometry [12] for the dominant modes at the time of maximum amplitude. Within the uncertainties due to the reduced spatial coverage, the modes peak at approximately the same location, as expected for efficient coupling.

Additional information on the the spatial relationship between mode amplitudes is available from the entire set of 11 Mirnov coils distributed toroidally over $360°$. By fitting the signal from the coils against the toroidal angle, the toroidal mode structures can be visualized along with their relative (toroidal) phase at a single time. The mode amplitude is represented as the deviation from the unitary radius circle of the fit as a function of the toroidal angle for each specific mode number. All mode amplitudes are rescaled by the same factor. The example given in Fig. 4d and detailed in Fig. 6 clearly shows that the $n = 1$ perturbation is generated by the overlap of positive and negative lobes of the $n = 4, 3$ modes, producing regions of constructive and destructive interference between mode pairs with a definite $n = 1$ structure. For this mechanism to be efficient, the modes must lock on the same Doppler shift (or rotation) frequency for a sufficiently long time, of the order of tens of wave cycles for the primary modes, as observed from the experiments.
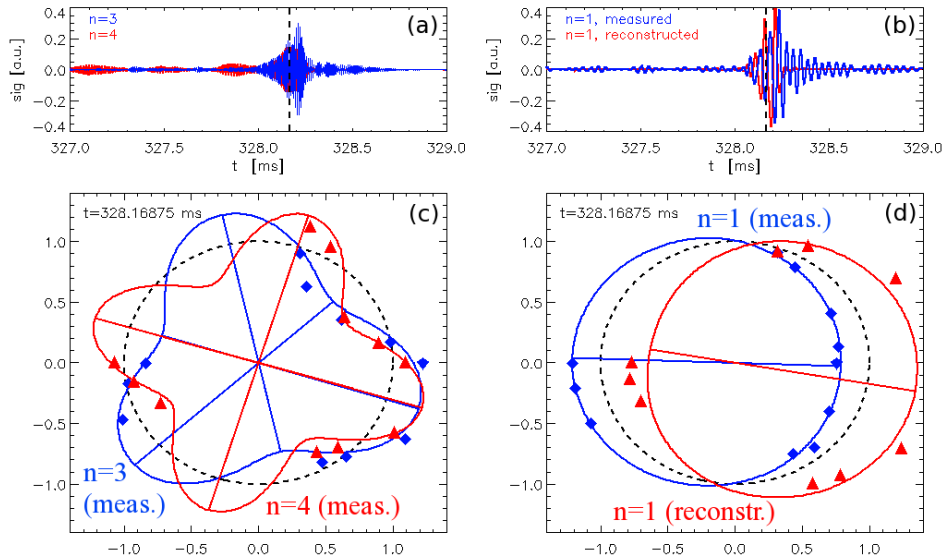
FIG. 6. (a) Measured rms amplitude of the $n = 3, 4$ modes from Mirnov coils data. (b) Measured and reconstructed (from quadratic interactions of $n = 3, 4$ modes) amplitude of the $n = 1$ mode. (c-d) Fit of the mode amplitude from 11 Mirnov coil sensors distributed toroidally vs toroidal angle for the modes in panels (a-b). Data refers to discharge no. 135414.

3. Discussion

In this work it has been shown that pairs of TAEs can efficiently couple and generate lower and higher frequency perturbations. The matching conditions for mode-mode coupling are verified for frequency, wave-number and phase of the primary and resulting modes. The coupling is transient, because the single-mode dynamics on short time scales leads to frequency and cross-phase variations that tend to invalidate the coupling conditions. However, when those conditions are met for 100's of microseconds, coupling can take place and the modes undergo a fast growth, which eventually lead to fast ion losses of $O(10\%)$ of the confined population. During this process the TAE amplitude grows by more than one order of magnitude over a few hundred microseconds. The *effective* growth rate $\gamma_{eff}/2\pi f)$, estimated experimentally from the nearly exponential increase of the mode amplitude, is $\gtrsim 10\%$, i.e. much larger than the typical linear growth rate of O(1%) calculated through the NOVA-K code [13] for TAEs on NSTX.

The strongest mode resulting from bilinear interactions is a $n = 1$ oscillation, which mediates the non-linear coupling between the primary TAEs. This mechanism is then different from other mode coupling processes previously observed on NSTX [14]. The nature of the $n = 1$ (and the weaker $n = 2$) low-frequency fluctuation remains an open question. Although the signal-to-noise of the reflectometer data is low (Fig. 5d), its structure peaks at the same location of that of the TAEs, around ≈ 132 cm. No data is available closer to the magnetic axis, $R \leq 120$ cm. According to Eq. 1, the mode frequency in the plasma frame is $f_0^{n=1} = f_{Doppler}^{TAE} - f_{Doppler}^{n=1}$. The more plausible interpretation is that $f_0^{n=1} \approx 0$ and $f_{Doppler}^{n=1} \approx f_{Doppler}^{TAE}$, i.e. the perturbation rotates rigidly with the TAE revolution frequency and is localized at similar radii as the primary TAEs. The spatial overlap between modes favors the coupling, and is in fact measured (*cf.* Fig. 5d) through the reflectometer system. Based on this information, two possibilities are left open: (i) the $n = 1$ perturbation is a forced oscillation (or a *quasi-mode*) driven by the large amplitude

primary TAEs, or (ii) it is an otherwise stable, kink-like plasma mode driven unstable by the coupling process. Further experiments with improved mode structure diagnostic capabilities (e.g. through Beam Emission Spectroscopy [15]) and a direct comparison with self-consistent, non-linear codes such as M3D-K ([16] and references therein) are foreseen to elucidate this issue.

[1] FASOLI, A., et al., Progress in the ITER physics basis: Chapter 5, Physics of energetic ions, Nucl. Fusion **47** (2007) S264.

[2] ONO, M., et al., Exploration of spherical torus physics in the NSTX device, Nucl. Fusion **40** (2000) 557.

[3] PODESTÀ, M., et al., Experimental studies on fast-ion transport by Alfvén wave avalanches on the National Spherical Torus Experimentt, Phys. Plasmas **16** (2009) 056104.

[4] FREDRICKSON, E. D., et al., Modeling fast-ion transport during toroidal Alfvén eigenmode avalanches in the National Spherical Torus Experiment, Phys. Plasmas **16** (2009) 122505.

[5] MEDLEY, S. S., et al., Mhd-induced energetic ion loss during h-mode discharges in the National Spherical Torus Experiment, Nucl. Fusion **44** (2004) 1158.

[6] WHITE, R. B., et al., Beam distribution modification by Alfvén modes, Phys. Plasmas **17** (2010) 056107.

[7] STRAIT, E. J., et al., Doppler shift of the TAE mode frequency in DIII-D, Plasma Phys. Control. Fusion **36** (1994) 1211.

[8] BELL, R. E., et al., Comparison of poloidal velocity measurements to neoclassical theory on NSTX, Phys. Plasmas **17** (2010) 082507.

[9] KIM, Y. B., et al., Neoclassical poloidal and toroidal rotation in tokamaks, Phys. Fluids B **3** (1991) 2050.

[10] PODESTÀ, M., et al., Effects of toroidal rotation shear on toroidicity-induced Alfvén eigenmodes in NSTX, Phys. Plasmas (submitted) (2010).

[11] KIM, Y. C., et al., Digital bispectral analysis and its applications to nonlinear wave interactions, IEEE Trans. Plasma Sci. **7** (1979) 120.

[12] CROCKER, N. A., et al., Alfvén cascade modes at high β in the National Spherical Torus Experiment, Phys. Plasmas **15** (2008) 102502.

[13] CHENG, C. Z., Kinetic extensions of magnetohydrodynamics for axisymmetric toroidal plasmas, Phys. Rep. 211 **1** (1992).

[14] CROCKER, N. A., et al., Three-wave interactions between fast-ion modes in the National Spherical Torus Experiment, Phys. Rev. Lett. **97** (2006) 045002.

[15] SMITH, D., et al., Design of the NSTX beam emission spectroscopy system and initial measurements, Rev. Sci. Instr. (2010) Proceedings of the 18th HTPD meeting, to be published.

[16] LANG, J., et al., Gyrokinetic ∂f particle simulations of toroidicity-induced Alfvén eigenmode, Phys. Plasmas **16** (2009) 102101.